SI APPENDIX

"Selective small molecule inhibitor of the *Mycobacterium tuberculosis* fumarate hydratase reveals an allosteric regulatory site"

Monica Kasbekar, Gerhard Fischer, Bryan T. Mott, Adam Yasgar, Marko Hyvönen, Helena I. M. Boshoff, Chris Abell, Clifton E. Barry III, and Craig J. Thomas

I. SI METHODS

Protein Expression and Purification

A pNAN plasmid containing N-terminal His_6-tagged *M. tuberculosis* fumarate hydratase (obtained from Dr. David Garboczi, National Institute of Allergy and Infectious Diseases) was transformed into *E. coli* Bl21(DE3) cells. The transformed host was grown for 16 h at 37 °C on lysogeny broth (LB) agar supplemented with 100 μg/mL ampicillin.

A single freshly transformed cell colony was grown in a starter culture (10 mL of LB media containing 100 μg/mL ampicillin) at 37 °C with shaking for 5 h. The starter culture was used to inoculate 1 L of LB media (100 μg/mL ampicillin), and the culture was grown at 37 °C with shaking to an OD_{600} of ∼0.6 before induction with 0.5 mM isopropyl-β-D-thiogalactopyranoside (IPTG). The temperature of the system was decreased to 15 °C, and the culture was grown for an additional 16 h. The cells were harvested by centrifugation (4,000 rpm, 20 min, 4 °C) using a Beckman Coulter Avanti J-20 XP centrifuge.

Cell pellets were resuspended in 10 mM imidazole in lysis buffer (50 mM Tris pH 8.0, 150 mM NaCl). Cells were lysed using a French press and centrifuged (16,000 rpm, 1 h, 4 °C). Chromatography was conducted using an Akta FPLC (GE Healthcare). The lysate was loaded onto a HisTrap^{TM}FF column (GE Healthcare) equilibrated with 10 mM imidazole in lysis buffer. The column was washed using 12 column volumes of 10 mM imidazole in lysis buffer, and the protein was eluted using a 20 column volume gradient of 10 mM to 1 M imidazole in lysis buffer. Fractions containing the fumarate hydratase protein were pooled and further purified on a Superdex 200 16/600 column (GE Healthcare), equilibrated with 10 mM Tris pH 8.0, 150 mM NaCl, and 0.5 mM TCEP. A centrifugal concentrator was used to yield purified protein, and the concentration was determined by amino acid analysis. Aliquots were flash-frozen in liquid nitrogen and stored at -80 °C until further use.

High-throughput Screen and Counterscreens

For the primary high-throughput screen, 3 μL of a (4/3)x solution containing all reagents except fumaric acid were dispensed into a 1,536-well Greiner black plate via a BioRAPTR dispenser (Beckman Coulter). 23 nL of compounds were single-pin transferred via a pin tool (Kalypsys) equipped with 1536 slotted pins (V&P Scientific). The plates were incubated for 10 min at room temperature. 1 μL of a 4x solution of fumaric acid was dispensed into the plate via the BioRAPTR dispenser. The plate was centrifuged for 15 s at 1,000 rpm and read immediately on a ViewLux High-throughput CCD imager (Perkin-Elmer) using a filter set with excitation at 525 nm and emission at 598 nm. The plate was read again after 5 min. The change in fluorescence intensity between the two reads was normalized against no-inhibitor and no-enzyme controls and the resulting percent inhibition data were plotted. Compounds were plated as four-point titrations as previously described [1, 2].

The citrate synthase counterscreen modified the primary high-throughput screening protocol in the following ways: (1) the citrate synthase and acetyl-CoA components were removed from the reagent mixture and (2) plates were imaged at a 20 min interval. The malate dehydrogenase counterscreen modified the primary protocol in the following ways: (1) the fumarate hydratase, citrate synthase, and acetyl-CoA components were removed from the reagent mixture and (2) in place of a 4x solution of fumaric acid, the reaction was initiated with a 4x solution of malic acid, to yield a final concentration of 40 μM. The diaphorase counterscreen modified the primary protocol in the following ways: (1) the fumarate hydratase, malate dehydrogenase, NAD^+, citrate synthase, and acetyl-CoA components were removed from the reagent mixture and (2) in place of a 4x solution of fumaric acid, the reaction was initiated with a 4x solution of NADH, to yield a final concentration of 15 μM.

Compound Characterization of N-(5-(azepan-1-ylsulfonyl)-2-methoxyphenyl)-2-(4-oxo-3,4-dihydrophthalazin-1-yl)acetamide (7)

LCMS analysis was performed using a Waters Aquity UPLC HClass LCMS. A 3.5 min runtime with a 2 min gradient of 5% to 95% acetonitrile in water containing 0.1% (v/v) formic acid was used. ^{1}H NMR and ^{13}C NMR spectra were recorded on a Bruker DPX 400 MHz spectrometer. Chemical shifts are reported in ppm relative to residual undeuterated DMSO from the DMSO-d_6 solvent. High-resolution mass spectrometry was recorded using a Waters LCT Premier high-resolution mass spectrometer using electrospray ionization in the positive mode.

Compound characterization of **7**: LCMS retention time: 1.90 min; ^{1}H NMR (400 MHz, DMSO-d_6): δ 12.62 (s, 1H), 9.86 (s, 1H), 8.46 (d, J = 2.2 Hz, 1H), 8.29 – 8.26 (m, 1H), 7.96-7.94 (m, 2H) 7.88-7.84 (m, 1H), 7.49 (dd, J = 8.7, 2.4 Hz, 1H), 7.24 (d, J = 8.7 Hz, 1H), 4.22 (s, 2H), 3.97 (s, 3H), 3.16-3.08 (m, 4H), 1.63-1.52 (m, 4H), 1.48-1.43 (m, 4H); ^{13}C NMR (125 MHz, DMSO-d_6) δ 168.3, 159.4, 152.0, 142.0, 133.5, 131.5, 130.4, 129.8, 127.6, 127.5, 125.9, 125.8, 123.4, 119.11, 119.10, 111.2, 56.3, 47.6 (2), 28.4 (2), 26.3 (2); HRMS (ESI) m/z (M+H)+ calcd. for $C_{23}H_{27}O_5N_4S$ 471.1697, found 471.1691.

Crystallization, Data Processing, and Structure Determination

For the formate-bound structure, crystallization trials were performed using a Crystal Phoenix crystallization robot (Art Robbins Instruments LLC) with the commercial screens JCSG+ (Qiagen), PEGS I (Qiagen), and Wizard (Emerald BioStructures). After screening and optimization of crystallization conditions, diffraction-quality crystals were exclusively obtained in crystallization conditions containing magnesium formate. Crystals were grown by sitting drop vapor diffusion at 20°C in 17.0% [w/v] PEG3350, 5% [v/v] DMSO, and 200 mM magnesium formate, by combining 2 μL of a 14 mg/mL protein solution with 1 μL of reservoir. The buffer composition of the protein solution was 10 mM Tris pH 8.0, 150 mM NaCl, and 0.5 mM TCEP.

For the **7**-bound crystals, both co-crystallization trials and soaking were attempted. Co-crystallization screens were also performed using a Crystal Phoenix crystallization robot (Art Robbins Instruments LLC) with the commercial screens JCSG+ (Qiagen), PEGS I (Qiagen), and Wizard (Emerald BioStructures). Co-crystallization screening and optimiza-

tion trials did not yield diffraction-quality crystals. Soaking experiments were conducted with the formate-bound crystals. Diffraction-quality crystals were obtained from soaking of the formate-bound crystals, by adding 2 μL containing a saturated solution of **7** in 19% PEG3350 [w/v], 7.5% [v/v] DMSO, and 200 mM magnesium formate to the sitting drop.

X-ray data were collected at a wavelength of 0.969 Å at beamline I24 and at 0.979 Å at beamline I04 of the Diamond Light Source synchrotron (Oxfordshire, United Kingdom). Both structures were solved by molecular replacement using PHASER [3]. The unbound *M. tuberculosis* fumarate hydratase (PDB ID: 3NO9) was used as a search model for the formate-bound structure, and the formate-bound structure was used as a search model for the **7**-bound structure. For the formate-bound structure, automated model rebuilding was performed using Buccaneer [4] followed by manual rebuilding and refinement in Coot [5]. The **7**-bound structure was manually rebuilt in Coot, based on the molecular replacement solution from PHASER. Structures were refined using Refmac5 [6] in the CCP4 program suite [7] and the Phenix suite [8], with 5% of the reflections excluded from refinement for R_{free} calculations.

Some of the residues from the N- and C-termini of each subunit and from the loop of residues 315 – 323 were omitted from the models due to missing electron density. For the formate-bound structure, missing residues are as follows – subunit A: -20 – 9 and 473 – 474; subunit B: -20 – 9, 15 – 16, and 473 – 474; subunit C: -20 – 6, 317 – 322, and 467 – 474; subunit D: -20 – 7, 317 – 323, and 470 – 474. For the **7**-bound structure, missing residues are as follows – subunit A: -20 – 8, 15 – 18, 316 – 323, and 468 – 474; subunit B: -20 – 9, 14 – 19, and 468 – 474; subunit C: -20 – 8, 315 – 324, and 467 – 474; subunit D: -20 – 17, 315 – 323, and 467 – 474. Although the N-termini of both structures are disordered, they do not appear to have any influence on the observed conformational changes. Ligand densities for **7** are clearly observed, except for the distal side of the cycloheptanyl substituent, which is disordered. Ramachandran statistics calculated with Molprobity [9] show no outliers, with 2.6% in allowed and 97.4% in Ramachandran favored regions for the formate-bound structure and no outliers, with 2.2% in allowed and 97.8% in favored regions for the **7**-bound structure. Coordinates and structure factors for the formate-bound structure and the complex with **7** have been deposited in the Protein Data Bank under accession numbers 5F92 and 5F91, respectively.

Human Fumarate Hydratase Selectivity

30 μL of a (4/3)x solution containing all reagents except fumaric acid was added to a 384-well plate. 1 μL of compound or vehicle was added, and the plate was incubated at room temperature for 10 minutes. 10 μL of a 4x solution of fumaric acid was added to the plate. The plate was centrifuged for 15 s at 1,000 rpm and read every 15 seconds in kinetic mode on a PHERAstar microplate reader (BMG Labtech) for 30 minutes using a filter set with excitation at 550 nm and emission at 590 nm.

Assessment of Colony-Forming Units of *M. tuberculosis* H37Rv under Anaerobic Conditions

Non-replicating persistence (NRP)-2 cultures of *M. tuberculosis* strain H37Rv were obtained by diluting early log phase cultures 100-fold in Dubos medium (Difco) and placing them in wax-sealed bottles with a head:space ratio of 0.5 for three weeks as previously described [10]. Cultures were opened and further manipulation was performed in an anaerobic chamber (MACS MG 1000 Anaerobic Workstations, Don Whitley Scientific) maintained under an atmosphere of 10:10:80 H_2:CO_2:N_2. In a 24-well plate, 980 μL of culture was added to 20 μL of drug or vehicle. The fumarate hydratase inhibitor was tested at concentrations of 200 μM, 50 μM and 12.5 μM. The metronidazole control was dosed at 100 μM, and the isoniazid control was dosed at 10 μg/mL. The plate was incubated in the anaerobic chamber at 37°C for 7 days. Cells were diluted by 10^3 and 10^4, and 100 μL was plated onto 10 cm 7H11-agar containing plates. The plates were incubated at 37°C for 5 weeks and then viable colonies were counted.

II. SI TABLES

	Fumarate hydratase with formate bound	Fumarate hydratase with **7** bound
PDB-code	5F92	5F91
Data Collection		
Space group	C2	C2
Cell dimensions		
a / b / c [Å]	180.1 / 97.0 / 124.1	175.2 / 96.5 / 124.4
α / β / γ [°]	90 / 103.4 / 90	90 / 102.7 / 90
Resolution [Å]	42.4-1.86 (1.865-1.859)*	60.7-2.00 (2.004-1.998)*
No. of reflections (all/unique)	585408 / 173375	382642 / 130081
R_{merge}	0.060 (0.553)	0.074 (0.506)
R_{meas}	0.071 (0.656)	0.090 (0.620)
I/σI	13.8 (2.1)	13.0 (2.1)
$CC_{1/2}$	0.998 (0.726)	0.997 (0.705)
Completeness [%]	99.4 (99.8)	95.1 (62.5)
Redundancy	3.4 (3.4)	2.9 (2.9)
Refinement		
Resolution [Å]	40.3-1.86	48.8-2.00
No. of reflections used	173353	130054
R_{work} / R_{free}	14.3 / 18.1	15.1 / 19.4
No. of atoms		
Protein	13693	13263
Formate	12	3
Inhibitor **7**		66
Water	1594	1549
B-factors		
Protein	26.7	25.5
Formate	25.5	28.3
Inhibitor **7**		27.5
Water	35.0	32.9
R.m.s deviations		
Bond lengths [Å]	0.011	0.007
Bond angles [°]	1.19	0.986

*Values for highest resolution shell are shown in parentheses

TABLE S1. **Data collection and refinement statistics for the fumarate hydratase structures.**

[Inhibitor **7**] (μM)	Apparent V_{max} (μM/min/mg enzyme)	Apparent K_m (mM)
28.6	160	67
14.3	160	17
7.2	160	4.7
3.6	160	1.4
1.8	160	0.590
0.9	160	0.360
0.4	160	0.290
0	160	0.260

TABLE S2. **Apparent $\mathbf{V}_{max}$ and $\mathbf{K}_m$ values for the curve fits shown in Fig. 3d.**

III. SI FIGURES

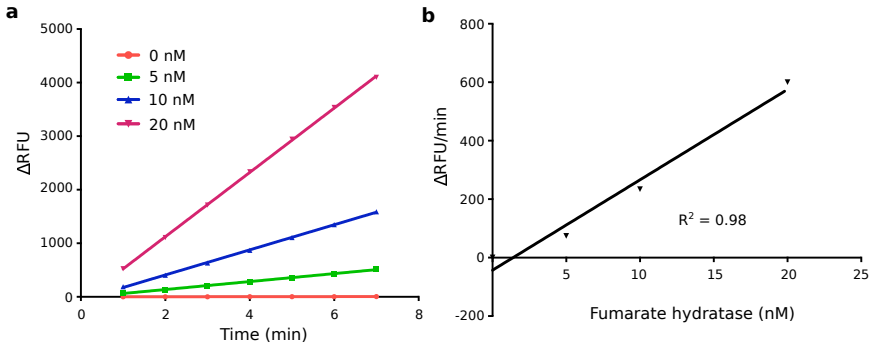

FIG. S1. **Validation of the high-throughput screening assay.** (a) The fluorescence output of the primary high-throughput screening assay measured at different concentrations of fumarate hydratase. Fluorescence production is linear for the first seven minutes at enzyme concentrations below 20 nM. Data are reported as an average of replicates (n=64) and error bars indicate s.e.m. (b) The initial reaction rate in the assay plotted as a function of fumarate hydratase concentration. The initial rate changes proportionally with changes in enzyme concentration below 20 nM. Linearity indicates that the assay is accurately monitoring fumarate hydratase activity.

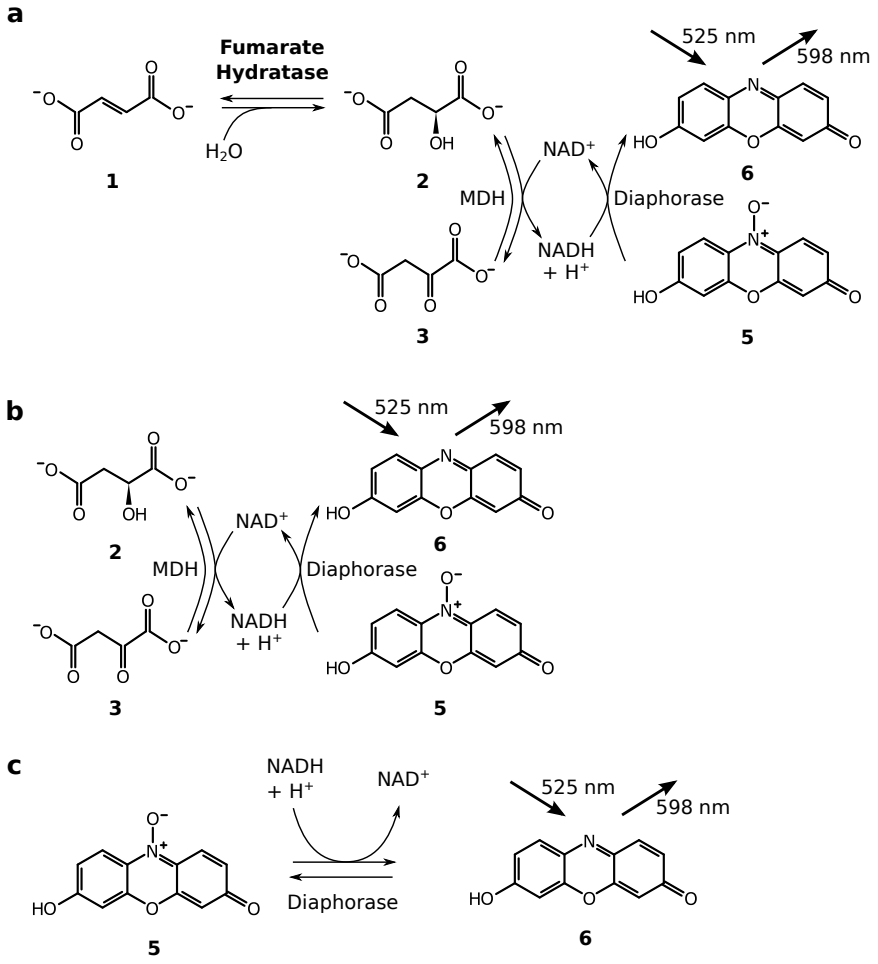

FIG. S2. **Counterassays used to eliminate compounds affecting other assay components.** (a) Schematic of the fluorescence-based counterassay used to eliminate compounds affecting citrate synthase activity. The assay mimics the primary high-throughput screening assay, but lacks citrate synthase and acetyl-CoA. (b) Schematic of the fluorescence-based counterassay used to eliminate compounds affecting malate dehydrogenase activity. (L)-malate (**2**) is used to initiate the reaction, and oxaloacetate (**3**) is produced. The assay is monitored by measuring the conversion of resazurin (**5**) to resorufin (**6**). (c) Schematic of the fluorescence-based counterassay used to eliminate compounds affecting diaphorase activity. NADH is used to initiate the reaction, and the assay is monitored by measuring the conversion of resazurin (**5**) to resorufin (**6**).

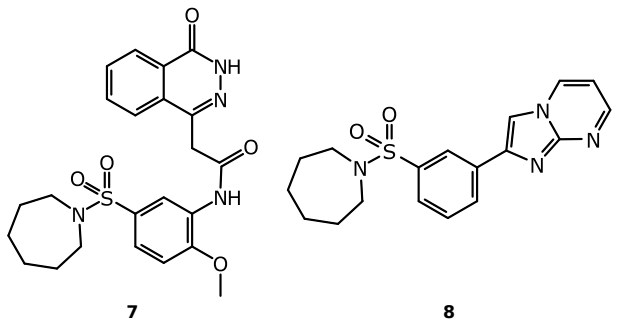

FIG. S3. **The structures of two compounds that were identified in the high-throughput screen.** The similarities between **7** and **8** resulted in further investigation of the more potent compound, **7**.

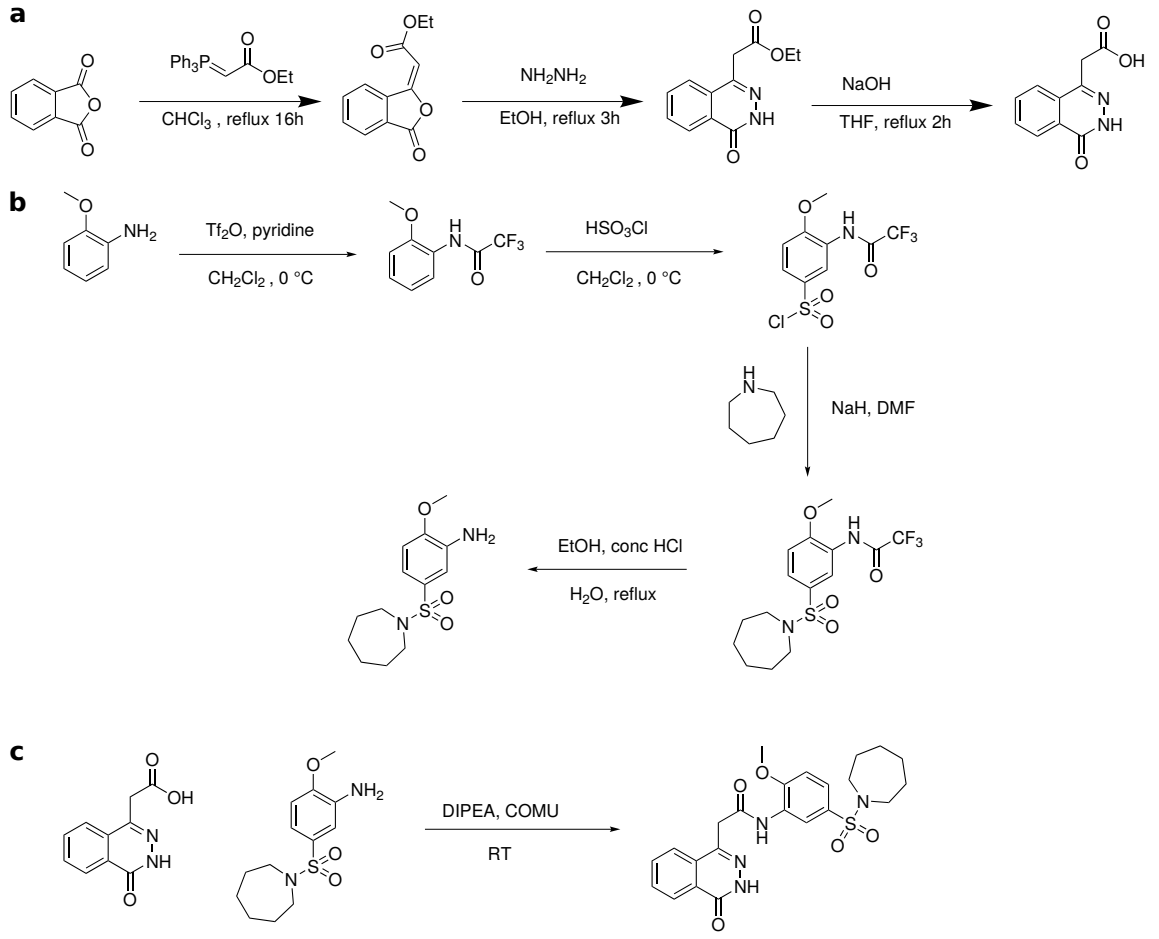

FIG. S4. **The synthetic scheme for resynthesis of 7.** (a) Synthetic scheme for 2-(4-oxo-3,4-dihydrophthalazin-1-yl)acetic acid [11]. (b) Synthetic scheme for 5-(azepan-1-ylsulfonyl)-2-methoxyaniline [12]. (c) Amide coupling reaction to generate **7** [13]. Final compound characterization data is provided in the SI Methods.

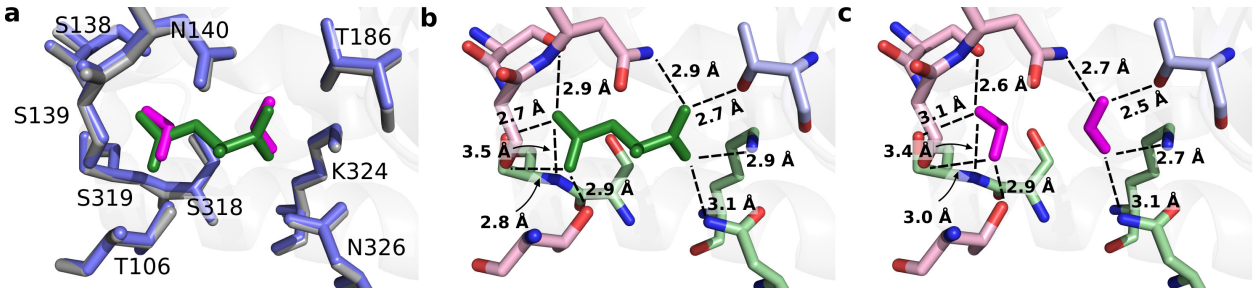

FIG. S5. **Formate ions mimic the binding mode of (L)-malate in the fumarate hydratase active site.** (a) The superimposition of the formate-bound fumarate hydratase active site residues (blue) with those of the (L)-malate bound structure (gray, PDB ID: 4ADL). The formate ions are shown in magenta, and the (L)-malate is shown in green. The carboxylates of (L)-malate superimpose with the formate ions. (b) Interactions made by the carboxylates of (L)-malate with residues in an enzyme active site. (c) The interactions of the formate ions with residues in an enzyme active site. The formate ions make the same contacts as the carboxylates of (L)-malate. Residues are colored according to subunit (light green: subunit A, light purple: subunit C, pink = subunit D), and residues from three of four subunits contribute to each active site.

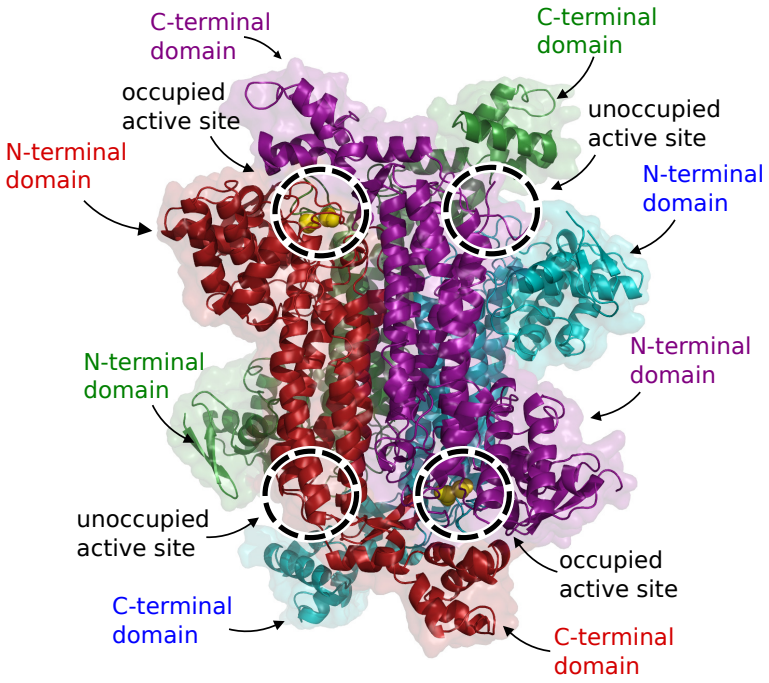

FIG. S6. **The relative positions of the formate-bound and unoccupied active sites within the fumarate hydratase tetramer.** Two of the four fumarate hydratase active sites (dashed circles) are occupied with substrate-mimicking formate ions (represented as yellow spheres). The active sites nearest to the C-terminal domains of subunits C and D contain formate ions. The remaining two active sites, nearest to the C-terminal domains of subunits A and B, are unoccupied. The binding of formate in only two of the four active sites is most likely due to crystal packing forces, as previously suggested [14]. Colors represent the subunits of the tetramer (green: subunit A, blue: subunit B, purple: subunit C, red: subunit D).

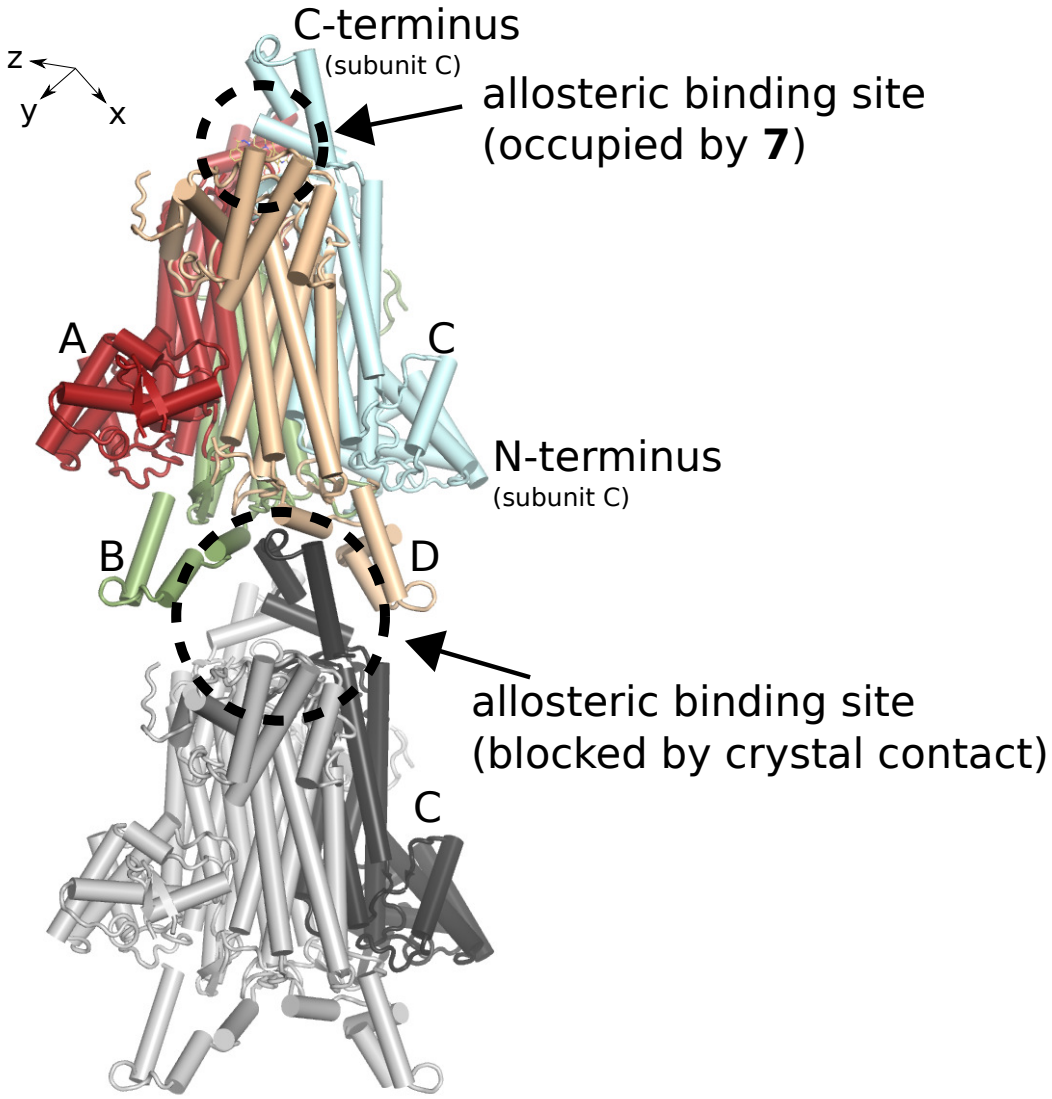

FIG. S7. **Crystal contact between two symmetry-related fumarate hydratase tetramers.** While the allosteric binding site between the C-termini of subunits A (red) and C (light blue) is occupied by two molecules of **7** (yellow, stick representation), the putative allosteric binding site between subunits B (green) and D (light orange) is occupied by the C-terminus of subunit C (dark grey) of a symmetry-related molecule (light grey), preventing the binding of **7** at this site.

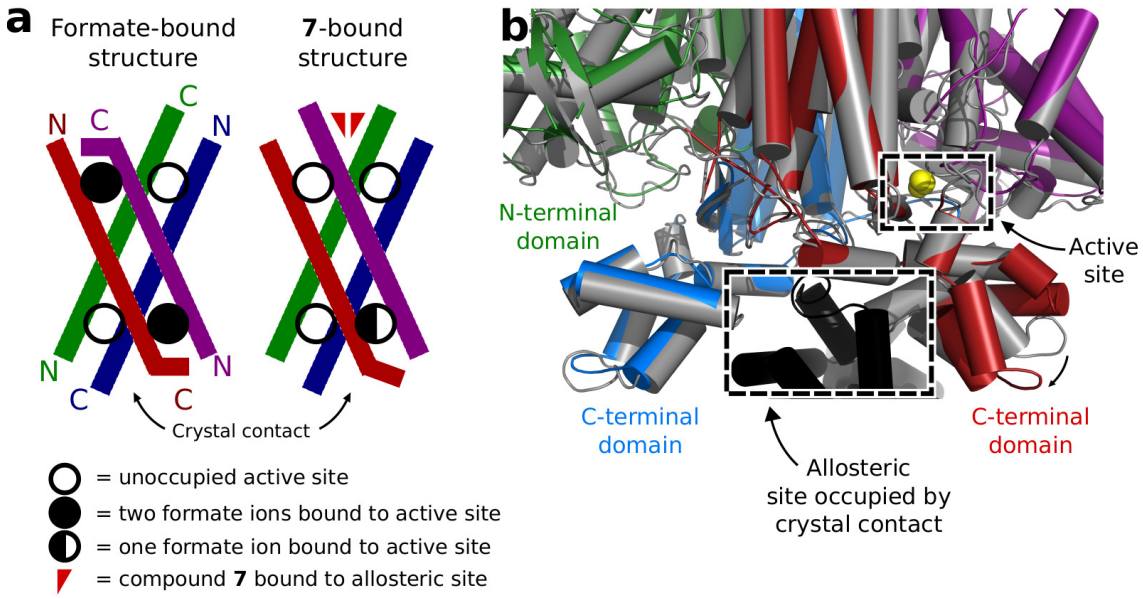

FIG. S8. **The active sites adjacent to each allosteric site.** (a) A cartoon representation showing the location of bound formate ions in each active site in both the formate-bound and the **7**-bound structure. Each subunit is represented by a different color (green: subunit A, blue: subunit B, purple: subunit C, red: subunit D), and the C-terminal and N-terminal domains are labeled with a 'C' or 'N', respectively. In the formate-bound structure, two of four active sites are occupied by formate ions. In the **7**-bound structure, the active site adjacent to **7** loses the electron density for both formate ions. The active site adjacent to the crystal contact loses the electron density for one of two formate ions. The loss of this one additional formate ion near the crystal contact could be due to crystal packing effects resulting from the change in the unit cell length. (b) Superimposition of the fumarate hydratase enzyme bound with formate (gray) or **7** (colored). In the **7**-bound structure, the allosteric site between the C-termini of subunits B (blue) and D (red) is occupied by a crystal contact with a symmetry-related fumarate hydratase tetramer (black). A rotation in the C-terminal domain of subunit D results in the loss of the electron density for one of two formate ions in the adjacent active site. The one remaining formate ion is depicted as a yellow sphere. Subunits A and C are depicted in green and purple, respectively.

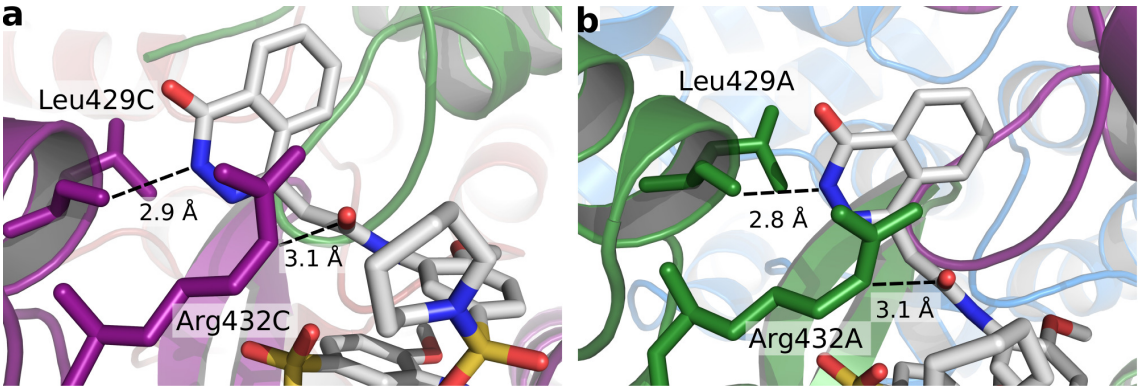

FIG. S9. **Identical protein-ligand interactions are observed for each of the two molecules of 7.** (a) Arg432 and Leu429 on protein subunit C make stacking and hydrogen bonding interactions with one of the molecules of **7**. (b) Identical interactions involving Arg432 and Leu429 on protein subunit A are observed with the other molecule of **7**.

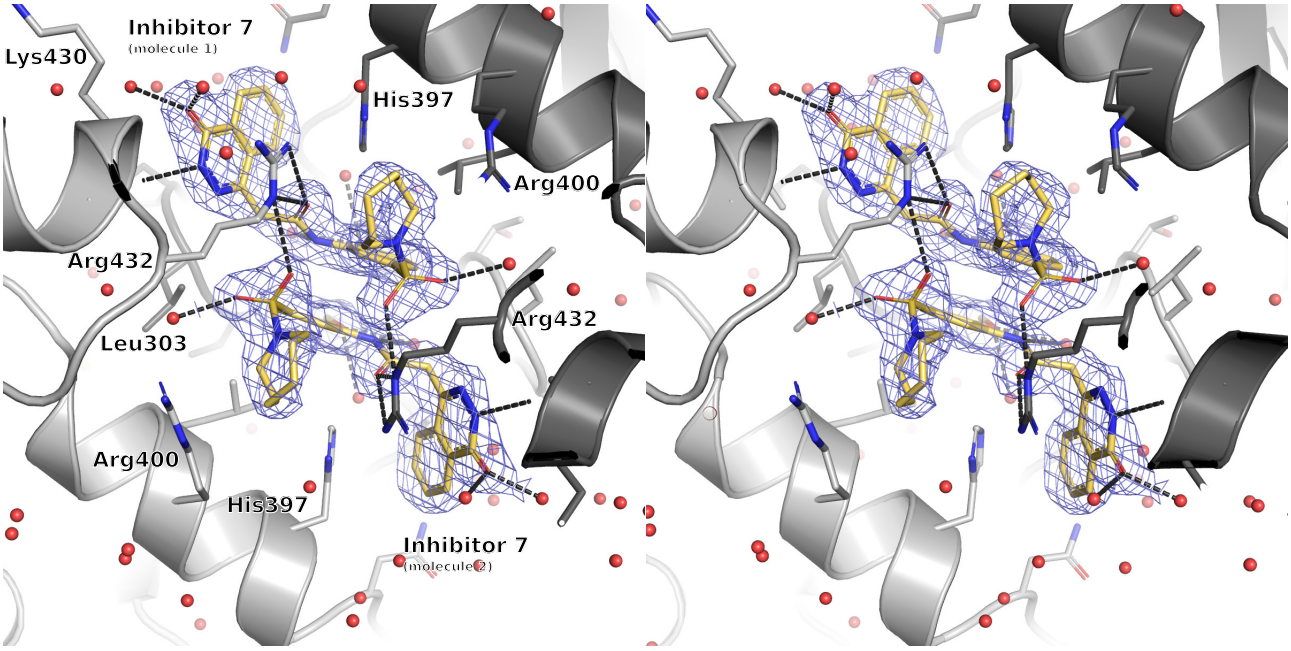

FIG. S10. **Stereoimage of the inhibitors in their electron density.** A stereoimage of the electron density surrounding the allosteric site, showing the bound inhibitors. Subunit A (light grey) and subunit C (dark grey) of the tetrameric complex form a new binding pocket, where two molecules of inhibitor **7** bind. Hydrogen bonds made by the inhibitor with surrounding amino acids and solvent molecules are shown as dashed lines.

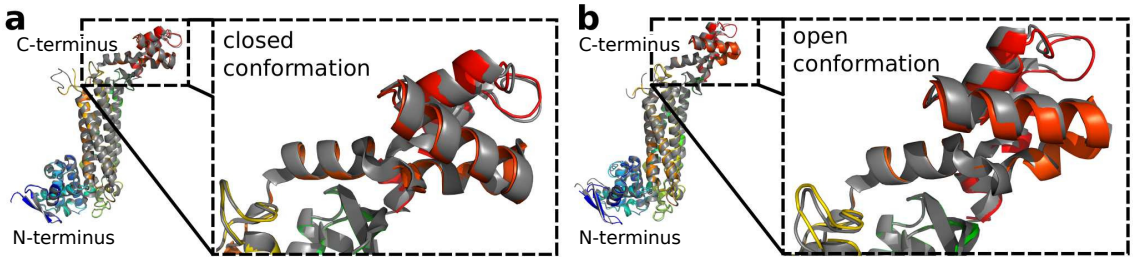

FIG. S11. **The 'closed' and 'open' enzyme conformations of the** *M. tuberculosis* **fumarate hydratase.** (a) Superimposition of a fumarate hydratase subunit from a structure bound with (L)-malate (gray; PDB ID: 4ADL) or formate (colored) in the nearest active site. In both structures, the C-terminal domain adopts the 'closed' conformation associated with substrate binding. (b) Superimposition of a fumarate hydratase subunit from the unbound structure (gray; PDB ID: 3NO9) or with **7** bound to the adjacent allosteric site (colored). When **7** is bound, the subunit is locked in the 'open' conformation, unable to participate in substrate binding.

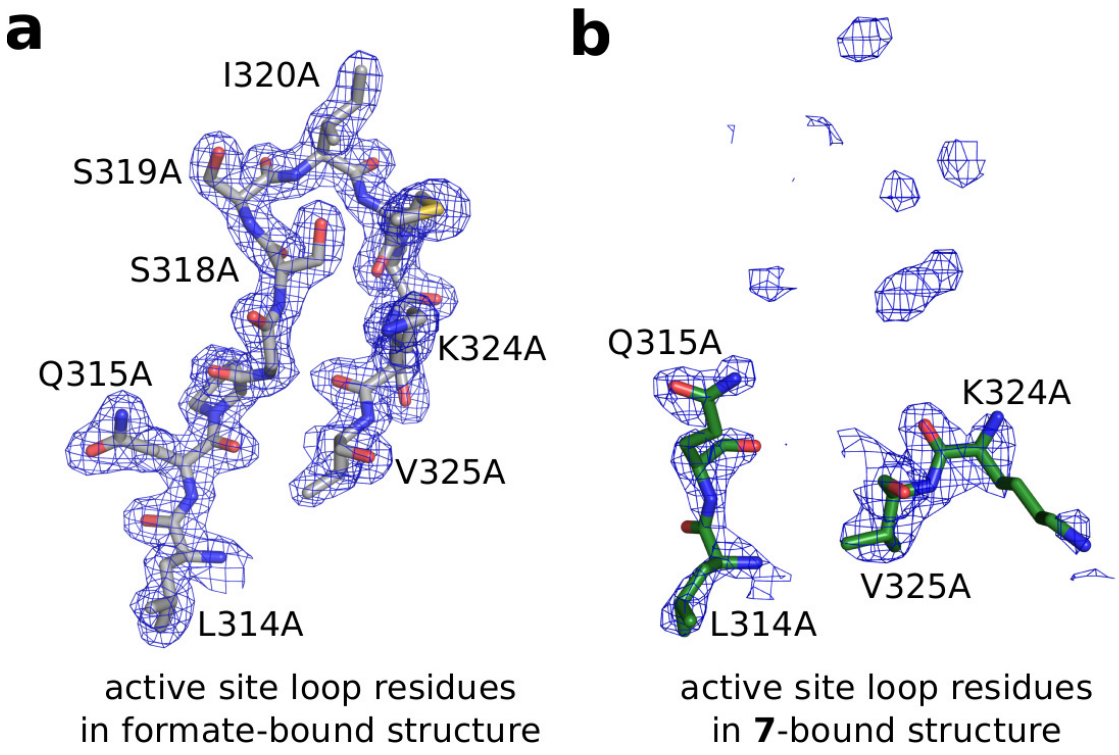

FIG. S12. **Electron density of active site loop residues is lost upon binding of 7.** (a) The electron density surrounding loop residues 314A-325A in the formate-bound structure. The portion of the $2F_o$ - F_c electron density map is depicted as a blue mesh and contoured at 1σ. Ser318A, Ser319A, and Lys324A are key active site residues that form hydrogen bonds with the formate ions. (b) In the structure with **7** bound, the electron density surrounding residues 316A-323A is lost, and these residues cannot be modeled.

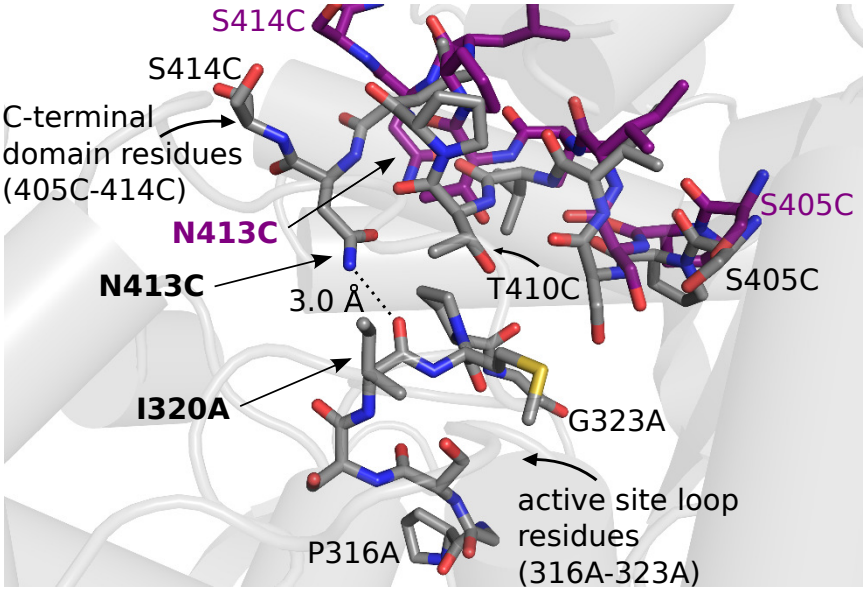

FIG. S13. **Hydrogen bond interaction stabilizes loop residues in the enzyme active site.** In the 'closed' conformation when formate is bound (gray), a stabilizing hydrogen bond is formed between a C-terminal domain residue (Asn413C) and the backbone oxygen atom of an active site loop residue (Ile320A). This interaction is lost upon movement of the C-terminal domain into the 'open' conformation (purple), and the active site loop residues 316A-323A can no longer be modeled.

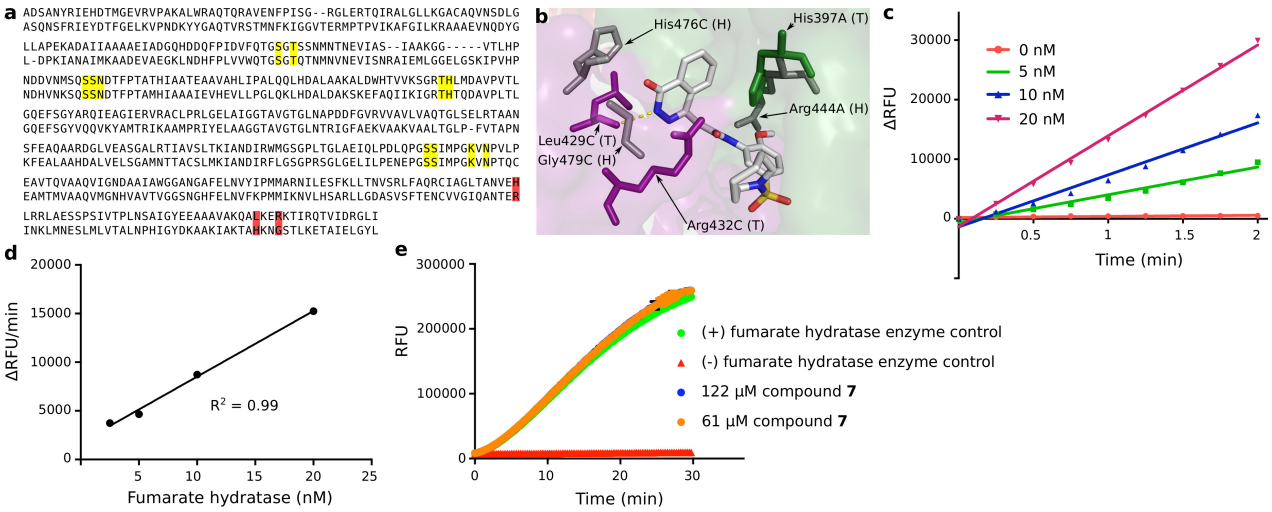

FIG. S14. **Compound 7 demonstrates selectivity over the human fumarate hydratase.** (a) The sequence alignment of the *M. tuberculosis* fumarate hydratase (top) and the human fumarate hydratase (bottom) as determined by the Standard Protein Basic Local Alignment Search Tool developed by the National Center for Biotechnology Information. Active site residues are highlighted in yellow, and allosteric site residues are highlighted in red. (b) A superimposition of the residues in the *M. tuberculosis* fumarate hydratase (color) and the human fumarate hydratase (gray, PDB ID: 3E04) at the location of the allosteric site. (c) The fluorescence output of the high-throughput screening assay measured at different concentrations of human fumarate hydratase. Fluorescence production is linear at enzyme concentrations below 20 nM. Data are reported as an average of replicates (n=2) and error bars indicate s.e.m. (d) The initial reaction rate in the human fumarate hydratase assay plotted as a function of enzyme concentration. The initial rate changes proportionally with changes in enzyme concentration below 20 nM. Linearity indicates that the assay is accurately monitoring human fumarate hydratase activity. (e) The reaction progress curves for human fumarate hydratase in the presence of varying concentrations of inhibitor **7**. The presence of **7** does not affect the progress of the reaction.

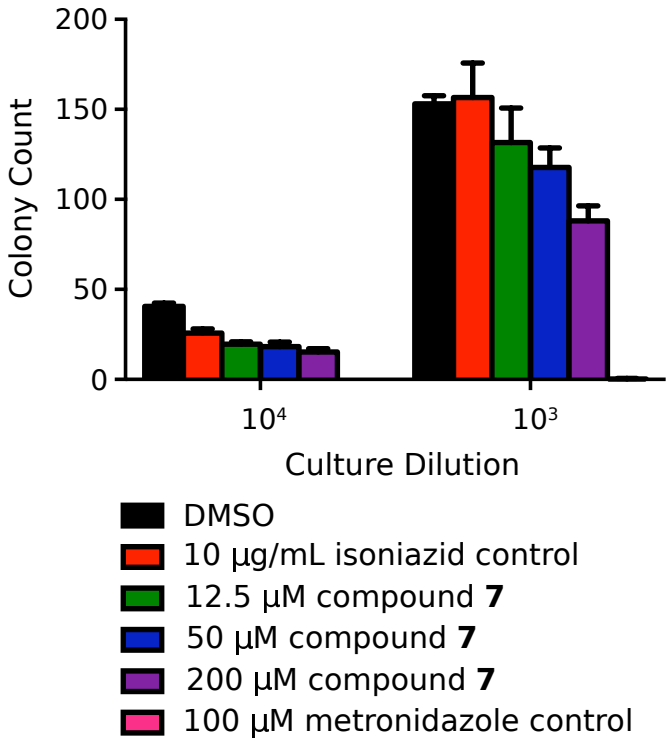

FIG. S15. **Treatment of *M. tuberculosis* H37Rv cells with the fumarate hydratase inhibitor 7 under anaerobic conditions does not demonstrate a significant effect on bacterial growth.** Controls include a DMSO-treated culture (black), an isoniazid-treated negative control (red), and a metronidazole-treated positive control (pink). Data are represented as an average of replicates (n=4) and error bars indicate s.e.m.

IV. SI REFERENCES

[1] Yasgar A, et al. (2008) Compound management for quantitative high-throughput screening. *J. Lab. Autom.* 13:79–89.

[2] Inglese J, et al. (2006) Quantitative high-throughput screening: a titration-based approach that efficiently identifies biological activities in large chemical libraries. *PNAS* 103:11473–11478.

[3] McCoy AJ, et al. (2007) *Phaser* crystallographic software. *J. Appl. Crystallogr.* 40:658–674.

[4] Cowtan K (2006) The *Buccaneer* software for automated model building. 1. Tracing protein chains. *Acta Crystallogr. D* 62:1002–1011.

[5] Emsley P, Cowtan K (2004) *Coot*: model-building tools for molecular graphics. *Acta Crystallogr. D* 60:2126–2132.

[6] Murshudov GN, et al. (2011) *REFMAC5* for the refinement of macromolecular crystal structures. *Acta Crystallogr. D* 67:355–367.

[7] Winn MD, et al. (2011) Overview of the *CCP4* suite and current developments. *Acta Crystallogr. D* 67:235–242.

[8] Adams PD, et al. (2010) *PHENIX*: a comprehensive Python-based system for macromolecular structure solution. *Acta Crystallogr. D* 66:213–221.

[9] Chen VB, et al. (2009) *MolProbity*: all-atom structure validation for macromolecular crystallography. *Acta Crystallogr. D* 66:12–21.

[10] Wayne LG, Hayes LG (1996) An in vitro model for sequential study of shiftdown of *Mycobacterium tuberculosis* through two stages of nonreplicating persistence. *Infect. and Immun.* 64:2062–2069.

[11] Johnson CR, et al. (2013) Phthalazinone inhibitors of inosine-5'-monophosphate dehydrogenase from *Cryptosporidium parvum*. *Bioorgan. Med. Chem.* 23:1004–1007.

[12] Nirogi R, et al. (2012) Design, synthesis, and pharmacological evaluation of piperidin-4-yl amino aryl sulfonamides: novel, potent, selective, orally active, and brain penetrant 5-HT6 receptor antagonists. *J. Med. Chem.* 55:9255–9269.

[13] El-Faham A, Funosas RS, Prohens R, Albericio F (2009) COMU: A safer and more effective replacement for benzotriazole-based uronium coupling reagents. *Chem–Eur. J.* 15:9404–9416.

[14] Mechaly AE, et al. (2012) Conformational changes upon ligand binding in the essential class II fumarase Rv1098c from *Mycobacterium tuberculosis*. *FEBS Lett.* 586:1606–1611.